Ultramicroscopy 150 (2015) 1–9

Contents lists available at ScienceDirect

Ultramicroscopy

journal homepage: www.elsevier.com/locate/ultramic

Adaptive and robust statistical methods for processing near-field scanning microwave microscopy images

K.J. Coakley [a,*], A. Imtiaz [a], T.M. Wallis [a], J.C. Weber [a,b], S. Berweger [a], P. Kabos [a]

[a] National Institute of Standards and Technology, Boulder, CO 80305, USA
[b] University of Colorado at Boulder, Boulder, CO 80309, USA

ARTICLE INFO

Article history:
Received 1 August 2014
Received in revised form
29 October 2014
Accepted 16 November 2014
Available online 23 November 2014

Keywords:
Adaptive weights smoothing
Atomic force microscopy
Denoising
Ferrite materials
Gwyddion
GaN nanowire
Leveling
Micro-capacitance calibration image
Near-field scanning probe microwave microscopy
Local regression and likelihood
Robust statistical methods
Scan artifacts
Statistical image processing

ABSTRACT

Near-field scanning microwave microscopy offers great potential to facilitate characterization, development and modeling of materials. By acquiring microwave images at multiple frequencies and amplitudes (along with the other modalities) one can study material and device physics at different lateral and depth scales. Images are typically noisy and contaminated by artifacts that can vary from scan line to scan line and planar-like trends due to sample tilt errors. Here, we level images based on an estimate of a smooth 2-d trend determined with a robust implementation of a local regression method. In this robust approach, features and outliers which are not due to the trend are automatically downweighted. We denoise images with the Adaptive Weights Smoothing method. This method smooths out additive noise while preserving edge-like features in images. We demonstrate the feasibility of our methods on topography images and microwave $|S_{11}|$ images. For one challenging test case, we demonstrate that our method outperforms alternative methods from the scanning probe microscopy data analysis software package Gwyddion. Our methods should be useful for massive image data sets where manual selection of landmarks or image subsets by a user is impractical.

Published by Elsevier B.V.

1. Introduction

Near-field scanning microwave microscopy (NSMM) offers great potential to facilitate characterization, development and modeling of materials. In NSMM, broadband microwave measurements and atomic force microscopy topography measurements at the nanometer scale are simultaneously acquired [1–7]. The simultaneous acquisition of microwave measurements and topography measurements is enabled by the integration of a one-port microwave signal path with a conventional atomic force microscope. The magnitude of the reflected microwave signal ($|S_{11}|$) is measured with a vector network analyzer. A review of the NSSM experimental technique is presented in [8]. Experimental applications include studies of dopants and defects in nanowires [9–11] and semiconductors [12–15,17]; characterization of wavelength-dependent conductivity and localized depletion regions in photovoltaics [18–20]; and cellular imaging and DNA studies of biological materials [21–24].

Images are acquired by scanning a sample line by line. Each scan line corresponds to a row (or column) in the acquired image. In order to maximize NSMM sensitivity at any operational frequency, that frequency is selected to be near the nearby frequency which yields the local minimum of the magnitude of the reflected microwave signal. One drawback of this strategy is that mechanical noise perturbs the location of microwave cabling and other instrument components, and hence produces artifacts in the acquired microwave signal that vary from scan line to scan line. In the simplest case, this source of error could introduce an additive offset that varies from scan line to scan line. Impurities or charging effects can also yield artifacts. Due to sample tilt errors, images can be distorted by planar (or nearly planar) trends. Moreover, additive noise obscures signals of interest. The focus of this paper is on robust and adaptive statistical methods to detrend, denoise and remove artifacts from measured images.

In particular, we focus on robust [25,26] and adaptive implementations of local regression [27–29] and local likelihood models [29–31] to detrend and denoise images. These methods are very flexible because they do not require explicit knowledge of a

* Corresponding author.

http://dx.doi.org/10.1016/j.ultramic.2014.11.014
0304-3991/Published by Elsevier B.V.

global parametric model. Instead, a local model is fit to a neighborhood about each location of interest. For instance, for 2-d images, the model could be a piece-wise constant, a plane or a quadratic surface. The size of the neighborhood is adjustable and influences results.

Topography images are typically distorted due to sample tilt errors. Some commonly used methods require the user to select a subset of the image for analysis and fit some model to this subset. For instance, in the software package Gwyddion [32], the subset could be a few landmarks or a larger fraction of the observed image with a user-selected mask. In contrast to these image subset methods, the modern statistical methods presented here are less subjective for two reasons. First, they do not require that the user specify an image subset or landmarks. Second, these models are fit to any observed image in a robust manner where large (in magnitude) residuals about the trend due to features of interest or outliers are automatically downweighted. In this work, we implement a robust version of the local regression method LOCFIT [29] to estimate smooth 2-d trends in images.

There are many methods to smooth noise in images [33]. However, simple methods such as 2-d kernel smoothing and median filtering smooth noise at the expense of blurring edge-like features in images. One can denoise images with a variety of methods designed to preserve edge-like features with more sophisticated methods including non-linear diffusion [34,35], wavelets [36], curvelets [37], contourlets [38], bandlets [39], and Adaptive Weight Smoothing [40–43]. Here, we denoise images and remove artifacts with the Adaptive Weights Smoothing (AWS) method which is a local likelihood method. In this approach, local models are fit by a weighted likelihood approach where the weights are adaptively determined for a variable size neighborhood about any point of interest. Since the weights can drop to zero near abrupt jumps in an image, this approach can preserve sharp features while suppressing additive noise in regions where the "true" image is smooth.

We illustrate our methods for atomic force microscopy topography and microwave $|S_{11}|$ images acquired from a micro-capacitor calibration sample, a GaN nanowire, and a ferrite material. Note that the atomic force microscope topography images are acquired in contact mode with the tip apex in direct contact with the sample. Typical image scan times are about 10 min. For this wide variety of examples, our approach dramatically suppresses artifacts, noise, and trends while preserving features of interest. For a very noisy ferrite material, we demonstrate that our approach dramatically outperforms an alternative approach based on methods in the software package Gwyddion. Although we focus on NSMM, the methods presented have broad applications in raster and scanning probe imaging modalities including: laser microscopy [44–46], scanning coherent anti-Stokes Raman microscopy [47], and Raman spectroscopy [48–50], luminescence imaging [51–53], fluorescent imaging and single molecule spectroscopy [54,55], photo acoustic molecular imaging [56], nonlinear sum frequency generation imaging [57–59], and aberration-corrected scanning transmission electron microscopy [60].

2. Methods

In this work, we level images, correct scan lines for offset artifacts, and denoise images. For leveling, we first estimate a smooth trend with a robust implementation of a local regression method called LOCFIT. At each point, we fit a local planar model where the neighborhood about each point is specified by a span parameter. In our approach, we set this span parameter to its maximal value of one. To suppress additive noise, this robust version of LOCFIT downweights large residuals by minimizing a bisquare cost function [25]. The scaling factor in the bisquare function is set to six times the median absolute residual. This robust fitting procedure is similar to the robust LOESS fitting procedure due to Cleveland [27].

We suppress scan line artifacts by subtracting the median measured value in any scan line from all measured values in that scan line. This correction method, available in Gwyddion, is plausible provided that the fraction of the scan due to features of interest is small (much less than 0.5) compared to a smooth background because the median estimate of a central value of a distribution of interest breaks down when over half of the observations are due to a contaminating source with a different distribution [25,26]. Similarly, our leveling method based on a robust fit of LOCFIT to 2-d images is appropriate when the fraction of the image occupied by features of interest is much less than 0.5.

We denoise and suppress artifacts with the AWS method. In the AWS method, the weighted likelihood function at point x is modeled as

$$L(W(x), \theta) = \sum_i w_i(x) \log p(Y_i, \theta), \tag{1}$$

where Y_i is measured at x_i, w_i is the weight corresponding to the measured value at x_i and the point of interest at x, p is the likelihood of Y_i given the model parameter vector θ. The basic idea of the AWS approach is to adaptively select the size of a neighborhood about any point of interest and the associated weights in that neighborhood. The overall smoothness of the image depends on the choice of a bandwidth parameter, h_{max}, that specifies the maximum size of any local neighborhood, and a parameter λ that determines when to stop expanding the size of the local neighborhood about any point according to a hypothesis test criterion. In general, as λ increases, the resulting image becomes smoother. Hence, λ can be regarded as an adjustable smoothing parameter.

Each image of interest is processed as follows:

- Estimate trend I_{trend} from observed image I_{obs} with robust implementation of LOCFIT.
- Get residual image $I_{res} = I_{obs} - I_{trend}$.
- Correct each scan line in I_{res} by subtracting corresponding median value in each scan line. Denote this row-corrected image as $I_{res,cor}$.
- Estimate LOCFIT trend for $I_{res,cor}$ and residual image, $I_{res,cor,*}$ about this trend.
- Smooth $I_{res,cor,*}$ with AWS algorithm to get final processed image $I_{process}$.

In general, detrending changes the mean value of an image. For the $|S_{11}|$ microwave images considered here, we add a constant to processed $|S_{11}|$ values so that mean values of the observed and processed images agree. For Atomic force microscopy (AFM) topography images, we subtract the minimum value from the processed image so that minimum value of processed image is zero.

For all applications of the AWS method here, we assume a Gaussian likelihood model for observations within each local neighborhood, and fit a local quadratic model about each point of interest. Further, we set the maximum size of each neighborhood h_{max} to 24.

Software for the LOCFIT and AWS algorithms described above is available from the public domain package **R** [61].

3. Examples

3.1. Capacitance image

We consider a very noisy topography image of a micro-

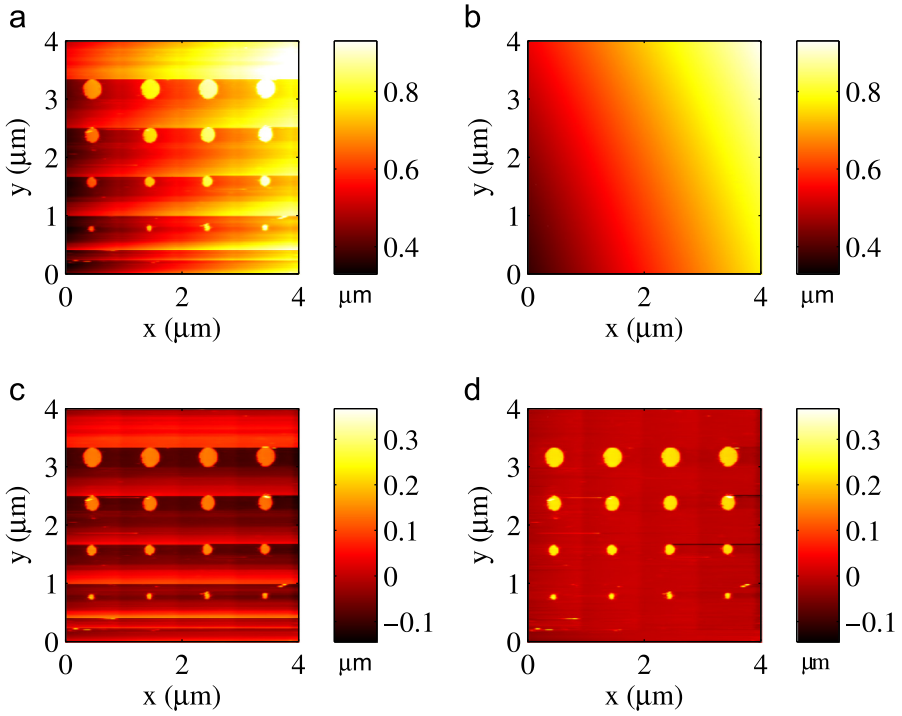

Fig. 1. Atomic force microscopy topography images of micro-capacitor calibration sample. (a) Observed. (b) Estimated smooth trend determined with LOCFIT method. (c) Residual image about trend. (d) Row-corrected and detrended version of (c).

capacitor calibration sample acquired by a NSMM with an AFM capability. In Fig. 1, we show the observed image I_{obs}, the LOCFIT trend estimate I_{trend}, the residual image I_{res}, and row-corrected and detrended image $I_{res,cor,*}$. In Fig. 2, we compare selected scan lines for I_{obs} and $I_{res,cor,*}$. In Fig. 3, we compare selected scan lines for I_{obs} and the processed image $I_{process}$. For the AWS algorithm, we assume a Gaussian likelihood function for the data. We increased the smoothing parameter λ to 1000 times its default value in order to suppress artifacts that we attribute to charging effects. As a caveat, this choice of λ is based on scientific judgement. In future work, we will investigate the feasibility of statistical learning methods [62] for selecting λ.

3.2. GaN nanowire

For a GaN nanowire, we acquire both an AFM topography image and a $|S_{11}|$ image at 18.5 GHz. The platinum tip of the instrument probe has a radius of curvature of approximately 20 nm. For smoothing, we assume a Gaussian likelihood model for the AFM topography and $|S_{11}|$ images and set the smoothing parameter λ in

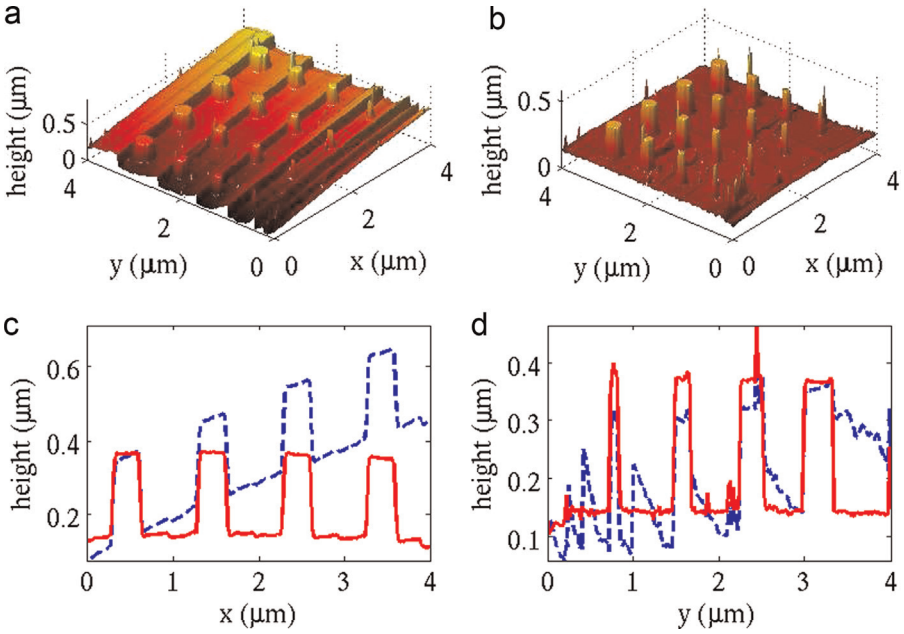

Fig. 2. Atomic force microscopy topography images of micro-capacitor calibration sample. (a) Observed (same data as shown in Fig. 1a). (b) Same data as shown in Fig. 1d. (c) Scan line comparison at $y = 3.28$ μm for (a). (d) Scan line comparison at $x = 0.47$ μm for (b). In (c) and (d) observed and processed results are plotted as dashed and solid lines respectively.

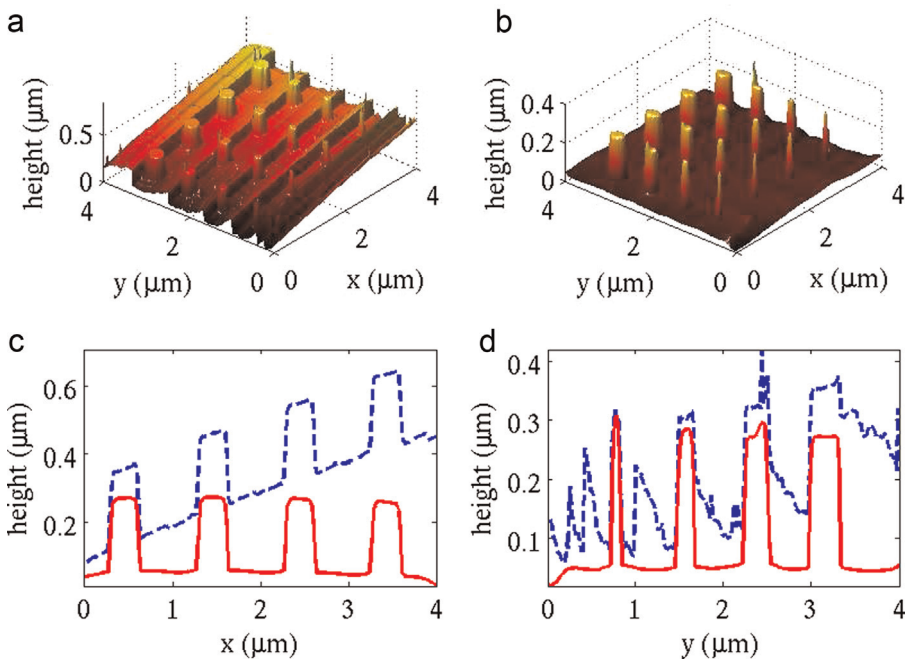

Fig. 3. Atomic force microscopy topography images of micro-capacitor calibration sample. (a) Observed (same data as shown in Fig. 1a). (b) Smoothed version of Fig. 1 (d) determined by the AWS method. (c) Scan line comparison at $y = 3.28$ μm for (a). (d) Scan line comparison at $x = 0.47$ μm for (b). In (c) and (d) observed and processed results are plotted as dashed and solid lines respectively.

the AWS algorithm to its default value.

Additive noise is clearly more significant in the $|S_{11}|$ image compared to the AFM topography measurement (Figs. 4 and 5). To illustrate how well the AWS method dramatically suppresses additive noise while preserving features of interest, we compare a scan line before and after denoising with the AWS method for the S_{11} image of the nanowire (Fig. 6).

The line-to-line variation of median observed values in the leveled $|S_{11}|$ image is visually more dramatic than the line-to-line variation of median observed values in the leveled AFM topography image (Fig. 7). Further, after correcting the leveled $|S_{11}|$ image (Figs. 5b) for a offset that varies line-to-line, band-like artifacts are significantly suppressed (Fig. 5c). In contrast, for the topography image, the leveled image (Fig. 4b) and image after correcting for line-to-line offsets (Fig. 4c) are, visually, very similar.

To quantify the observed variation of scan line medians, we define the following metrics:

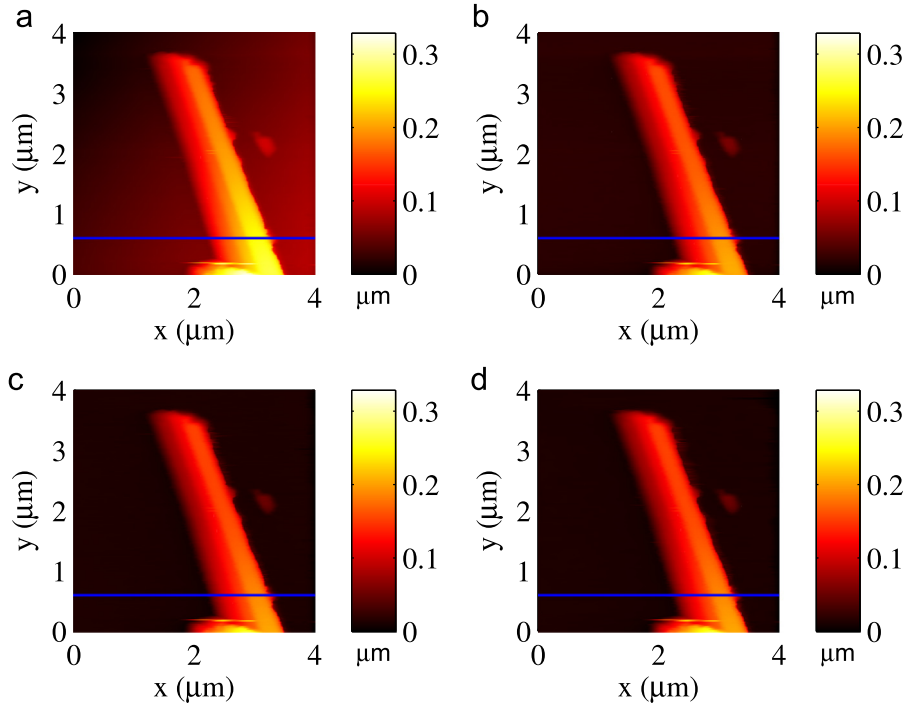

Fig. 4. Atomic force microscopy topography images of GaN nanowire. (a) Observed. (b) Leveled. (c) Leveled and corrected for scan offsets. (d) Leveled, corrected for scan offsets, and denoised.

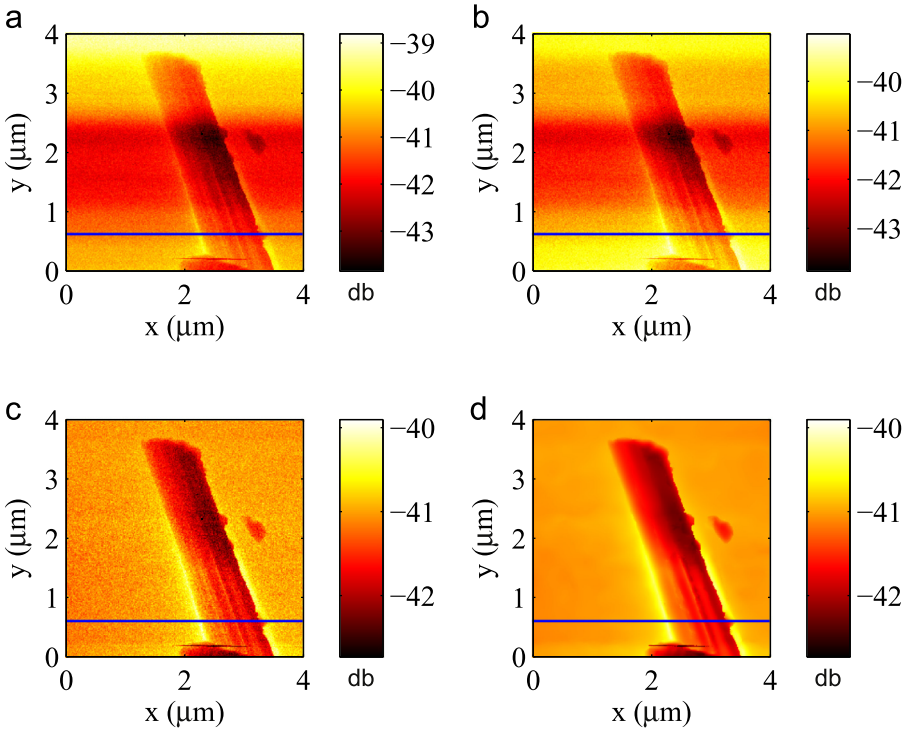

Fig. 5. $|S_{11}|$ images of GaN nanowire. (a) Observed. (b) Leveled. (c) Leveled and corrected for scan offsets. (d) Leveled, corrected for scan offsets, and denoised.

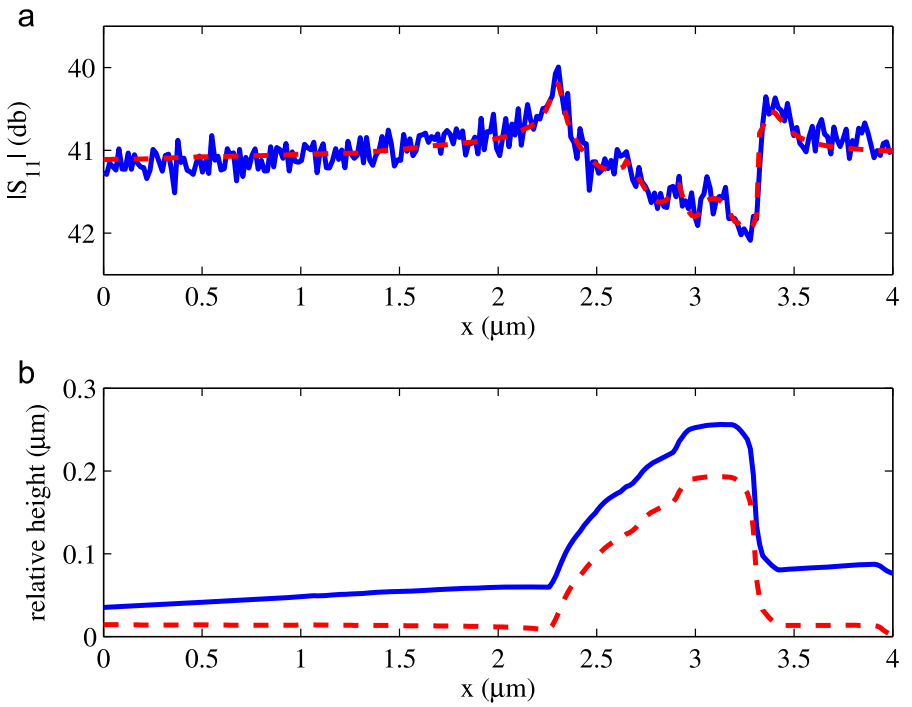

Fig. 6. (a) $|S_{11}|$ values before denoising (solid line), and after denoising (dashed line) along the scan line as shown in Fig. 5(c) and (d). (b) Observed (solid line) and processed atomic force microscope topography measurements (dashed line) corresponding to the scan line as shown in Fig. 4(a) and (d).

$$\Delta_{obs} = \frac{r_{max,obs} - r_{min,obs}}{I_{max} - I_{min}} \tag{2}$$

and

$$\Delta_{level} = \frac{r_{max,level} - r_{min,level}}{I_{max} - I_{min}}, \tag{3}$$

where $r_{min,obs}$ and $r_{max,obs}$ are the minimum and maximum values of the scan line medians for the observed image, $r_{min,level}$ and $r_{max,level}$ are the minimum and maximum values of the scan line medians for the leveled image, and I_{min} and I_{max} are the minimum and maximum value of the final processed image $I_{process}$. For the topography image, Δ_{obs} and Δ_{level} are 0.213 and 0.032 respectively. For the $|S_{11}|$ image, Δ_{obs} and Δ_{level} are 1.327 and 0.955 respectively. Thus, after leveling, the relative variation of the scan line medians for the $|S_{11}|$ image is approximately 30 times greater for the $|S_{11}|$ amplitude image relative to the topography image according to these metrics. As a caveat, the observed variation of scan line

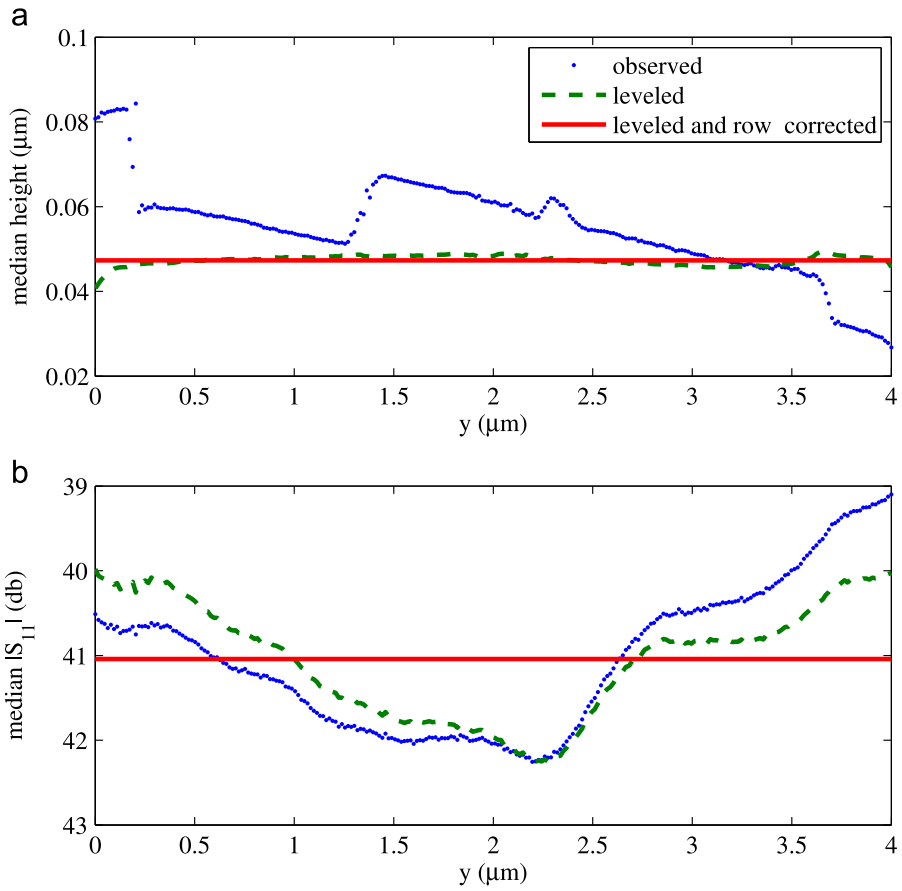

Fig. 7. (a) Median values of observed, leveled and row-corrected surface height values for each row of topography images (Fig. 4) of a GaN nanowire. (b) Median values of observed, leveled and row-corrected values for each row of $|S_{11}|$ images (Fig. 5) of a GaN nanowire.

medians could be due to the joint effect of instrumental artifacts and physical effects related to topographic and material variability.

There are common features in both the AFM topography and $|S_{11}|$ images. Comparison of a particular scan line demonstrates this point clearly (Fig. 8). As-grown GaN nanowires are known to have a hexagonal cross section, the observed $|S_{11}|$ scan lines in Fig. 8, display a series of local minima that we attribute to the presence of sharp topographic edges, including the edge of the nanowire as well as the boundaries between the facets on the surface of the wire. Our ultimate goal is to quantify material properties and

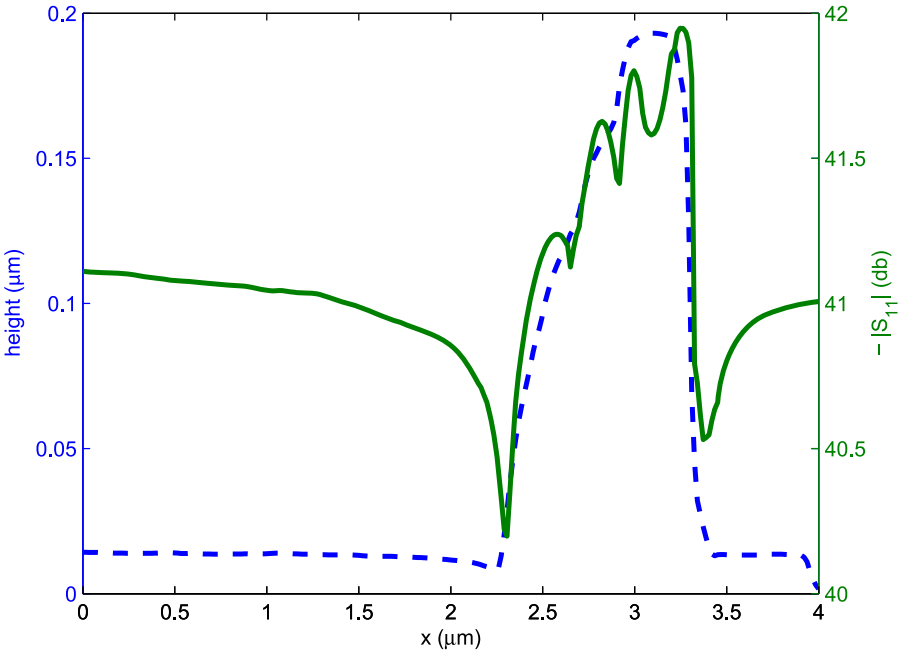

Fig. 8. Comparison of a scan line from processed topography (Fig. 4(d)) and $|S_{11}|$ (Fig. 5(d)) images of a GaN nanowire.

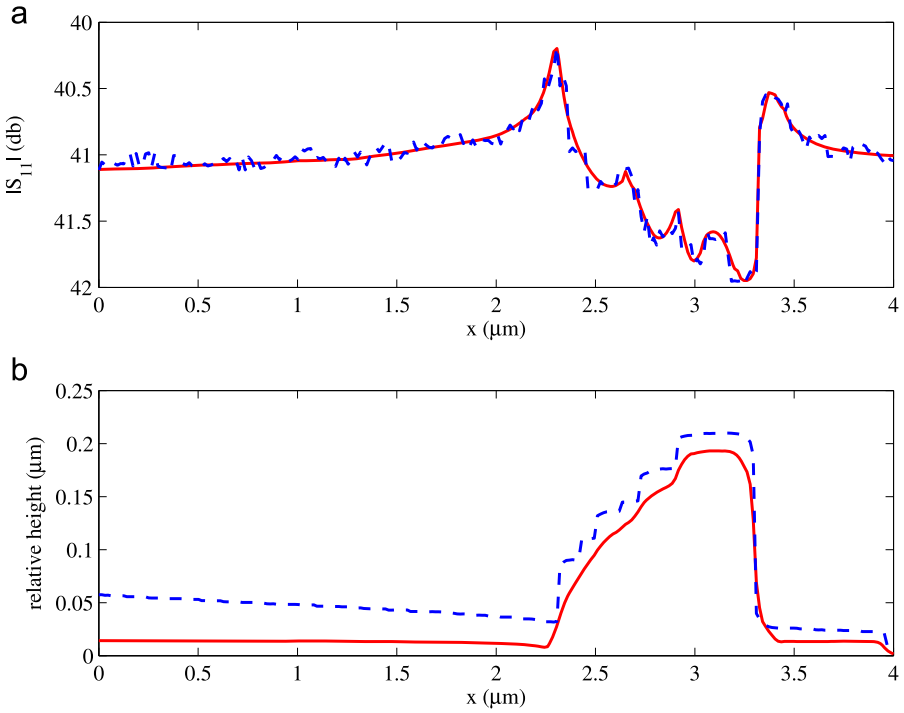

Fig. 9. Comparison of NIST and Gwyddion methods for processing GaN images. (a) Processed microwave S_{11} images according to NIST (solid line) and Gwyddion (dashed line). (b) Processed atomic force microscope topography images according to NIST (solid line) and Gwyddion (dashed line) methods.

device physics based on both topography and microwave measurements. Hence, understanding the dependence of measured $|S_{11}|$ on both topographic variations and material property variations is a key, and ongoing, research topic.

In Fig. 9, we compare results determined with our methods for detrending, denoising and artifact removal with those obtained by Gwyddion. In the Gwyddion approach, leveling is based on a planar trend fit to the full image. Row-to-row offsets are estimated based on the median value in each row. Finally, the image is denoised with the edge-preserving Kuwahara filter [63]. For the microwave S_{11} measurement (Fig. 9(a)), compared to Gwyddion, our methods appear to yield somewhat sharper and less noisy results for the region where there are a series of local minima. For other regions, our method appear to smooth out noise much better than the Gwyddion method. For the atomic force

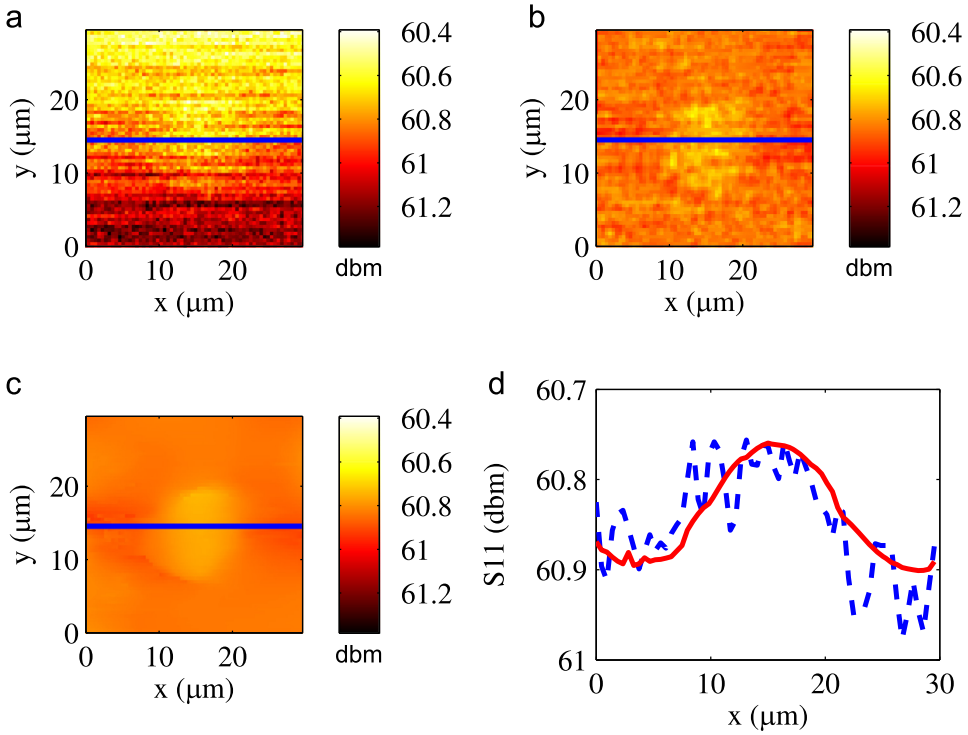

Fig. 10. $|S_{11}|$ images for a ferrite material. (a) Observed. (b) Processed version of (a) based on Gwyddion software. (c) Processed version of (a) based on our methods. (d) Scan lines from (b) (dashed) and (c) (solid).

microscopy topography measurement, (Fig. 9(b)), the Gwyddion detrending method failed to level the image as well as our approach did. Furthermore, the Kuwahara denoising method appears to introduce sawtooth-like artifacts (Fig. 9(b)) not apparent in the raw AFM topography image (Figs. 4 and 6(b)).

3.3. Ferrite material

In Fig. 10, we compare an observed $|S_{11}|$ (Fig. 10a) image for a ferrite material and the associated processed image determined by the methods described in this paper (Fig. 10(c)). For comparison, we leveled, row-corrected and denoised the same observed image with software from the public domain package Gwyddion (Fig. 10b). Visually, our methods yield superior results compared to Gwyddion. As a caveat, for microwave S_{11} images less noisy than the considered here, the difference between our methods and those in Gwyddion may not, in general, be as dramatic. Further, for the example considered, there surely are more effective edge preserving denoising methods to compare with the AWS method than the Kuwahara filter method. Comparison of the AWS method with other methods such as wavelets is beyond the scope of this study.

4. Summary

For a variety of examples including a capacitance calibration sample, a GaN nanowire, and a ferrite material, we demonstrated that our adaptive and robust local regression method dramatically suppress artifacts, noise, and trends while preserving features of interest in both atomic force microscopy topography images and microwave S_{11} images acquired with an NSMM. In particular, we demonstrated the feasibility of a robust local regression method for determining smooth 2-d trends in NSMM images. In this robust approach, we estimated the smooth trend with LOCFIT from all measured values in a manner that automatically downweighted measured values due to outliers and features of interest. Unlike many other popular methods based on user-selected landmarks or subsets, we estimate a smooth trend from the entire image. Hence, the user need not select landmarks or image subsets. As a caveat, our approach is for cases where the fraction of the image occupied by features of interest is much less than 0.5. Our methods should be useful for massive image data sets where manual selection of landmarks or image subsets by a user is impractical. We also presented a new metric that quantifies the observed range of scan line offset artifacts that vary from line-to-line.

We demonstrated the feasibility of the AWS method for denoising and smoothing out artifacts for both AFM topography and microwave $|S_{11}|$ images. For a very noisy $|S_{11}|$ image of a ferrite material (Fig. 10) and for AFM topography and microwave $|S_{11}|$ images of a GaN nanowire (Fig. 9), we demonstrated that our approach outperformed an alternative approach from the software package Gwyddion that included denoising with the edge-preserving Kuwahara filter. In the LOCFIT and the AWS methods, we set adjustable parameters that control the overall smoothness of the processed image based on scientific judgement. In future work, we plan to research statistical learning methods [62] for automatically determining such parameters, and methods to quantify the random uncertainty associated with processed images.

For a GaN nanowire, topography and $|S_{11}|$ images revealed common features in both (Figs. 4 and 5). The observed $|S_{11}|$ scan lines in Fig. 8, displayed a series of local minima that we attribute to the presence of sharp topographic edges, including the edge of the nanowire as well as the boundaries between the facets on the surface of the wire. However, the AFM topography measurement did not resolve these local minima. (Figs. 4, 5 and 8). In general, we expect that NSSM measurements to vary with frequency as discussed in [3]. However, we expect the performance or our processing methods for detrending, denoising and artifact removal to be similar.

Our ultimate goal is to quantify material properties and device physics based on both topography and microwave measurements. Hence, understanding the dependence of measured $|S_{11}|$ on both topographic variations and material property variations is a key, and ongoing, research topic.

Acknowledgments

The contribution of staff of NIST, an agency of the US government, is not subject to copyright in the US. We thank N.A. Sanford of NIST for providing experimental data and K.A. Bertness of NIST for useful discussions.

References

[1] M. Tabib-Azar, Y. Wang, Design and fabrication of scanning near-field microwave probes compatible with atomic force microscopy to image embedded nanostructures, IEEE Trans. Microw. Theory Tech. 52 (3) (2004) 971.
[2] P. Huber, M. Moertelmaier, T.M. Wallis, C.J. Chiang, M. Hochleitner, A. Imtiaz, Y. J. Oh, K. Schilcher, M. Dieudonne, J. Smoliner, Calibrated nanoscale capacitance measurements using a scanning microwave microscope, Rev. Sci. Instrum. 81 (2010) 113701.
[3] A. Imtiaz, T.M. Wallis, S.H. Lim, H. Tanbakuchi, H.P. Huber, A. Hornung, P. Hinterdorfer, J. Smoliner, F. Kienberger, P. Kabos, Frequency-selective contrast on variably doped p-type silicon with a scanning microwave microscope, J. Appl. Phys. 111 (2012) 093727.
[4] C. Gao, X.D. Xiang, Quantitative microwave near-field microscopy of dielectric properties, Rev. Sci. Instrum. 69 (1998) 3846.
[5] L. Zhang, Y. Ju, A. Hosoi, A. Fujimoto, Microwave atomic force microscopy imaging for nanometer-scale electrical property characterization, Rev. Sci. Instrum. 81 (2010) 123708.
[6] M. Farina, D. Mencarelli, A. Di Donato, G. Venanzoni, A. Morini, Calibration protocol for broadband near-field microwave microscopy, IEEE Trans. Microw. Theory Tech. 59 (2011) 2769.
[7] J.C. Weber, P.T. Blanchard, A.W. Sanders, A. Imtiaz, T.M. Wallis, K.J. Coakley, K. A. Bertness, P. Kabos, N.A. Sanford, V.M. Bright, Gallium nitride nanowire probe for near-field scanning microwave microscopy, Appl. Phys. Lett. 104 (2014) 023113.
[8] S.M. Anlage, V.V. Talanov, A.R. Schwartz, Principle of near field microwave microscopy, in: Scanning Probe Microscopy: Electrical and Electromechanical Phenomenon at the Nanoscale, Springer-Verlag, New York, 2007, pp. 215–253.
[9] K. Kim, T.M. Wallis, P. Rice, C.-J. Chiang, A. Imtiaz, P. Kabos, D.S. Filipovic, A framework for broadband characterization of individual nanowires, IEEE Microw. Wirel. Compon. Lett. 20 (2010) 178.
[10] C.-J. Chiang, T.M. Wallis, D. Gu, A. Imtiaz, P. Kabos, P.T. Blanchard, K.A. Bertness, N.A. Sanford, K. Kim, D. Filipovic, High frequency characterization of a Schottky contact to a GaN nanowire bundle, J. Appl. Phys. 107 (2010) 124301.
[11] M. Wallis, D. Gu, A. Imtiaz, C.S. Smith, C.-J. Chiang, P. Kabos, P.T. Blanchard, N. A. Sanford, K.A. Bertness, Electrical characterization of photoconductive GaN nanowires from 50 MHz to 33 GHz, IEEE Trans. Nanotechnol. 10 (2011) 832–838.
[12] P. Budka, S.D. Waclawik, G.M. Rebeiz, A coaxial 0.5–18 GHz near electric field measurement system for planar microwave circuits using integrated probes, IEEE Trans. Microw. Theory Tech. 44 (1996) 2174.
[13] M. Tabib-Azar, P.S. Pathak, G. Ponchak, S. LeClair, Nondestructive superresolution imaging of defects and nonuniformities in metals, semiconductors, dielectrics, composites, and plants using evanescent microwaves, Rev. Sci. Instrum. 70 (1999) 2783.
[14] A. Imtiaz, S.M. Anlage, J.D. Barry, J. Melngailis, Nanometer-scale material contrast imaging with a near-field microwave microscope, Appl. Phys. Lett. 90 (2007) 143106.
[15] C. Plassard, E. Bourillot, J. Rossignol, Y. Lacroute, E. Lepleux, L. Pacheco, E. Lesniewska, Detection of defects buried in metallic samples by scanning microwave microscopy, Phys. Rev. B 83 (2011) 121409.
[17] P. Huber, I. Humer, M. Hochleitner, M. Fenner, M. Moertelmaier, C. Rankl, A. Imtiaz, T.M. Wallis, H. Tanbakuchi, P. Hinterdorfer, Calibrated nanoscale dopant profiling using a scanning microwave microscope, J. Appl. Phys. 111 (2012) 014301.
[18] A. Hovsepyan, A. Babajanyan, T. Sargsyan, H. Melikyan, S. Kim, J. Kim, K. Lee, B. Friedman, Direct imaging of photoconductivity of solar cells by using a near-field scanning microwave microprobe, J. Appl. Phys. 106 (2009) 114901.
[19] K. Kim, A. Babajanyan, T. Sargsyan, H. Melikyan, S. Kim, B. Friedman, K. Lee, Visualization of magnetic domains by near-field scanning microwave microscope, Ultramicroscopy 109 (2009) 958.

[20] J.C. Weber, J.B. Schlager, N.A. Sanford, A. Imtiaz, T.M. Wallis, L.M. Mansfield, K. J. Coakley, K.A. Bertness, P. Kabos, V.M. Bright, A near-field scanning microwave microscope for characterization of inhomogeneous photovoltaics, Rev. Sci. Instrum. 83 (2012) 083702.
[21] S. Kim, H. Yoo, K. Lee, B. Friedman, M.A. Gaspar, R. Levicky, Distance control for a near-field scanning microwave microscope in liquid using a quartz tuning fork, Appl. Phys. Lett. 86 (2005) 153506.
[22] M. Tabib-Azar, J.L. Katz, Evanescent microwaves: a novel super-resolution noncontact nondestructive imaging technique for biological applications, IEEE Trans. Instrum. Meas. 48 (1999) 1111.
[23] B. Friedman, M.A. Gaspar, S. Kalachikov, K. Lee, R. Levicky, G. Shen, H. Yoo, Sensitive, label-free DNA diagnostics based on near-field microwave imaging, J. Am. Chem. Soc. 127 (2005) 9666.
[24] M. Farina, A. Di Donato, T. Monti, T. Pietrangelo, T. Da Ros, A. Turco, G. Venanzoni, A. Morini, Tomographic effects of near-field microwave microscopy in the investigation of muscle cells interacting with multi-walled carbon nanotubes, Appl. Phys. Lett. 101 (2012) 203101.
[25] P.J. Huber, Robust Statistics, John Wiley and Sons, New York, 1981.
[26] F.R. Hampel, E.M. Ronchetti, P.J. Rousseeuw, andW.A. Stahel, Robust Statistics, The Approach Based on Influence Functions, John Wiley and Sons, New York, 1986.
[27] W.S. Cleveland, Robust locally weighted regression and smoothing scatterplots, J. Am. Stat. Assoc. 74 (1979) 829–836.
[28] W.S. Cleveland, S.J. Devlin, Locally weighted regression: an approach to regression analysis by local fitting, J. Am. Stat. Assoc. 83 (1988) 596–610.
[29] C. Loader, Local Regression and Likelihood, Springer, New York, 1999.
[30] R.J. Tibshirani, Local Likelihood Estimation (Ph.D. thesis), Department of Statistics, Stanford University, 1989.
[31] R.J. Tibshirani, T.J. Hastie, Local likelihood estimation, J. Am. Stat. Assoc. 82 (1987) 559–567.
[32] ⟨ttp://gwyddion.net/⟩.
[33] R.C. Gonzalez, R.E. Woods, Digital Image Processing, 3rd ed., Pearson Prentice Hall, New Jersey, 2008.
[34] J. Malik, P. Perona, Scale-space and edge detection using anisotropic diffusion, IEEE Trans. Pattern Anal. Mach. Intell. 12 (7) (1990) 629–639.
[35] J. Weickert, Anisotropic Diffusion in Image Processing. ECMI Series., Tuebner-Verlag, Stutgart, 1998.
[36] S. Mallat, A Wavelet Tour of Signal Processing, 2nd ed., Academic Press, Burlington, MA, 1998.
[37] E.J. Candes, D.L. Donoh, Curvelets: A Surprisingly Effective Nonadaptive Representation for Objects with Edges, Stanford University, Dept of Statistics, Stanford, CA, 2000.
[38] M.N. Do, M. Vetterli, The Contourlet transform: an efficient directional multiresolution image representation, IEEE Trans. Image Process. 14 (12) (2005) 2091–2106.
[39] E. Le Pennec, S. Mallat, Sparse geometrical image representation with bandlets, IEEE Trans. Image Process. 14 (4) (2005) 423–438.
[40] J. Polzehl, V. Spokoiny, Adaptive weights smoothing with applications to image restoration, J. R. Stat. Soc. Ser. B 62 (2) (2000) 335–354.
[41] J. Polzehl, V. Spokoiny, Image denoising: pointwise adaptive approach, Ann. Stat. 31 (2003) 30–57.
[42] J. Polzehl, V. Spokoiny, Propagation-separation approach for local likelihood estimation, Probab. Theory Relat. Fields 135 (3) (2006) 335–362.
[43] K. Tabelow, J. Polzehl, H.U. Voss, V. Spokoin, Analyzing fMRI experiments with structural adaptive smoothing procedures, NeuroImage 33 (1) (2006) 55–62.
[44] K. Carlsson, P.E. Danielsson, A. Liljeborg, L. Majlf, R. Lenz, N. slund, Three-dimensional microscopy using a confocal laser scanning microscope, Opt. Lett. 10 (1985) 53–55.
[45] Z. Xie, S. Jiao, H.F. Zhang, C.A. Puliafito, Laser-scanning optical-resolution photoacoustic microscopy, Opt. Lett. 34 (2009) 1771–1773.
[46] M.A. Digman, C.M. Brown, P. Sengupta, P.W. Wiseman, A.R. Horwitz, E. Gratton, Measuring fast dynamics in solutions and cells with a laser scanning microscope, Biophys. J. 89 (2) (2005) 1317–1327.
[47] M.D. Duncan, J. Reintjes, T.J. Manuccia, Scanning coherent anti-Stokes Raman microscope, Opt. Lett. 7 (8) (1982) 350–352.
[48] A. Hartschuh, E.J. Snchez, X.S. Xie, L. Novotny, High-resolution near-field Raman microscopy of single-walled carbon nanotubes, Phys. Rev. Lett. 90 (9) (2003) 095503.
[49] S. Keren, C. Zavaleta, Z. Cheng, A. de La Zerda, O. Gheysens, S.S. Gambhir, Noninvasive molecular imaging of small living subjects using Raman spectroscopy, Proc. Natl. Acad. Sci. 105 (15) (2008) 5844–5849.
[50] P.J. Treado, M.D. Morris, Infrared and Raman spectroscopic imaging, Appl. Spectrosc. Rev. 29 (1) (1994) 1–38.
[51] R.D. Grober, T.D. Harris, J.K. Trautman, E. Betzig, Design and implementation of a low temperature near field scanning optical microscope, Rev. Sci. Instrum. 65 (3) (1994) 626–631.
[52] F. Treussart, V. Jacques, E. Wu, T. Gacoin, P. Grangier, J.F. Roch, Photoluminescence of single colour defects in 50 nm diamond nanocrystals, Physica B: Condens. Matter 376 (2006) 926–929.
[53] O. Faklaris, et al., Detection of single photoluminescent diamond nanoparticles in cells and study of the internalization pathway, Small 4 (12) (2008) 2236–2239.
[54] Y. Durand, J.C. Woehl, B. Viellerobe, W. Ghde, M. Orrit, New design of a cryostat-mounted scanning near-field optical microscope for single molecule spectroscopy, Rev. Sci. Instrum. 70 (2) (1999) 1318–1325.
[55] F. Luisier, C. Vonesch, T. Blu, M. Unser, Fast haar-wavelet denoising of multidimensional fluorescence microscopy data, in: Proceedings of the Sixth IEEE International Symposium on Biomedical Imaging: From Nano to Macro (ISBI'09), Boston MA, USA, June 28–July 1, 2009, pp. 310–313.
[56] A. De La Zerda, et al., Carbon nanotubes as photoacoustic molecular imaging agents in living mice, Nat. Nanotechnol. 3 (9) (2008) 557–562.
[57] M. Danckwerts, L. Novotny, Optical frequency mixing at coupled gold nanoparticles, Phys. Rev. Lett. 98 (2) (2007) 026104.
[58] Y. Nakayama, P.J. Pauzauskie, A. Radenovic, R.M. Onorato, R.J. Saykally, J. Liphardt, P. Yang, Tunable nanowire nonlinear optical probe, Nature 447 (7148) (2007) 1098–1101.
[59] S. Palomba, M. Danckwerts, L. Novotny, Nonlinear plasmonics with gold nanoparticle antennas, J. Opt. A: Pure Appl. Opt. 11 (11) (2009) 114030.
[60] M. Varela, et al., Spectroscopic imaging of single atoms within a bulk solid, Phys. Rev. Lett. 92 (9) (2004) 095502.
[61] ⟨http://cran.us.r-project.org/⟩.
[62] T. Hastie, R.J. Tibshirani, J. Friedman, The Elements of Statistical Learning, Springer, New York, 2001.
[63] M. Kuwahara, K. Hachimura, S. Eiho, M. Kinoshita, Processing of RI-angiocardiographic images, in: K. Preston Jr., M. Onoe (Eds.), Digital Processing of Biomedical Images, Plenum, New York, 1976, pp. 187–202.